Mutation of an atypical oxirane oxyanion hole improves regioselectivity of the α/β-fold epoxide hydrolase Alp1U

Received for publication, August 10, 2020, and in revised form, September 25, 2020 Published, Papers in Press, October 1, 2020, DOI 10.1074/jbc.RA120.015563

Liping Zhang[1,2,‡], **Bidhan Chandra De**[1,3,‡], **Wenjun Zhang**[1,2,3,*], **Attila Mándi**[4], **Zhuangjie Fang**[1,3], **Chunfang Yang**[1,2], **Yiguang Zhu**[1,2,3], **Tibor Kurtán**[4], **and Changsheng Zhang**[1,2,3,*]

From the [1]Key Laboratory of Tropical Marine Bio-resources and Ecology, Guangdong Key Laboratory of Marine Materia Medica, Innovation Academy of South China Sea Ecology and Environmental Engineering, and South China Sea Institute of Oceanology, Chinese Academy of Sciences, Guangzhou, China, the [2]Southern Marine Science and Engineering Guangdong Laboratory (Guangzhou), Guangzhou, China, the [3]University of the Chinese Academy of Sciences, Beijing, China, and the [4]Department of Organic Chemistry, University of Debrecen, Debrecen, Hungary

Edited by Ruma Banerjee

Epoxide hydrolases (EHs) have been characterized and engineered as biocatalysts that convert epoxides to valuable chiral vicinal diol precursors of drugs and bioactive compounds. Nonetheless, the regioselectivity control of the epoxide ring opening by EHs remains challenging. Alp1U is an α/β-fold EH that exhibits poor regioselectivity in the epoxide hydrolysis of fluostatin C (compound 1) and produces a pair of stereoisomers. Herein, we established the absolute configuration of the two stereoisomeric products and determined the crystal structure of Alp1U. A Trp-186/Trp-187/Tyr-247 oxirane oxygen hole was identified in Alp1U that replaced the canonical Tyr/Tyr pair in α/β-EHs. Mutation of residues in the atypical oxirane oxygen hole of Alp1U improved the regioselectivity for epoxide hydrolysis on 1. The single site Y247F mutation led to highly regioselective (98%) attack at C-3 of 1, whereas the double mutation W187F/Y247F resulted in regioselective (94%) nucleophilic attack at C-2. Furthermore, single-crystal X-ray structures of the two regioselective Alp1U variants in complex with 1 were determined. These findings allowed insights into the reaction details of Alp1U and provided a new approach for engineering regioselective epoxide hydrolases.

Stereoselective hydrolytic opening of epoxide rings is attractive in asymmetric synthesis, because the resultant vicinal diols are valuable building blocks of chiral drugs and bioactive compounds (1, 2). In biological systems, epoxide hydrolases (EHs) are extensively studied to catalyze the cofactor-independent hydrolysis of epoxides to vicinal diols (3, 4). The enzymatic mechanisms of EHs have been well-characterized by substrate selectivity and crystal structures combined with molecular dynamics simulations and directed evolution approaches (5–9). Most EHs belong to members of a family with an α/β hydrolase-fold, sharing a catalytic core domain and a cap domain (10). The α/β-EHs usually feature a catalytic triad and an oxirane oxygen hole that enable a two-step mechanism involving an S_N2 reaction and ester hydrolysis (Fig. 1*A*) (10, 11). The catalytic triad contains two aspartates and one histidine (10). In the first step, the attack of the nucleophilic aspartate ion against the epoxide ring forms a covalently linked enzyme-acyloxy-substrate adduct (5, 6). In the second step, the His and the other Asp activate a water molecule to hydrolyze the enzyme-acyloxy-substrate intermediate and release the products as *trans*-vicinal diols (12, 13). The oxirane oxygen hole contains a pair of tyrosines, which are proposed to donate hydrogen bonds to the oxirane oxygen, thereby assisting the first step of reaction sequence by activating the epoxide and stabilizing the formed oxyanion (6, 14). Another family of EHs, represented by the limonene-1,2-epoxide hydrolases, catalyzes a one-step mechanism with S_N2 ring opening of the epoxide ring by an enzyme-activated water molecule (Fig. 1*B*) (15).

These EH-catalyzed epoxide ring–opening mechanisms generally follow the S_N2 type, with backside attack by the nucleophile resulting in inversion of stereoconfiguration at the reactive carbon center (6, 15). However, engineering control of the regioselectivity into the epoxide ring–opening reaction remains challenging for EHs (15, 16). In synthetic epoxide hydrolysis, the regioselectivity depends on the substituents on the epoxide carbons (17) and the strength of the nucleophilic reagent. However, in the EH-catalyzed epoxide ring–opening reactions, the regioselectivity is influenced more by the structure of the enzyme active site (18). These steric constraints can potentially also control the stereochemistry of the product. This hypothesis is supported by enzyme engineering of EHs by directed evolution strategy or small mutagenic library screening (15, 16, 19–21). Unfortunately, mechanistic details of what causes regioselectivity improvement of engineered EHs are still elusive.

In the biosynthesis of vicinal diols, the chirality of these functional natural products derived from oxiranes plays important roles toward directing of postmodifications of the hydroxy groups, such as acylation and glycosylation. Representative examples include the EH Nasvi-EH1 involved in the biosynthesis of an insect sex attractant (22), the α/β-EHs NcsF2 and SgcF-catalyzed epoxide ring opening in the biosynthesis of enediyne antitumor antibiotics neocarzinostatins and C-1027 (23, 24), the TsrI-mediated endopeptidyl hydrolysis and epoxide ring opening/macrocyclization in thiostrepton biosynthesis (25), and the Alp1U-catalyzed epoxide hydrolysis of epoxykinamycins (Fig. 1*C*) (26). Interestingly, we have shown that the Alp1U found in *Streptomyces ambofaciens* also uses fluostatin

This article contains supporting information.
‡These authors contributed equally to this work.
*For correspondence: Wenjun Zhang, wzhang@scsio.ac.cn; Changsheng Zhang, czhang2006@gmail.com.

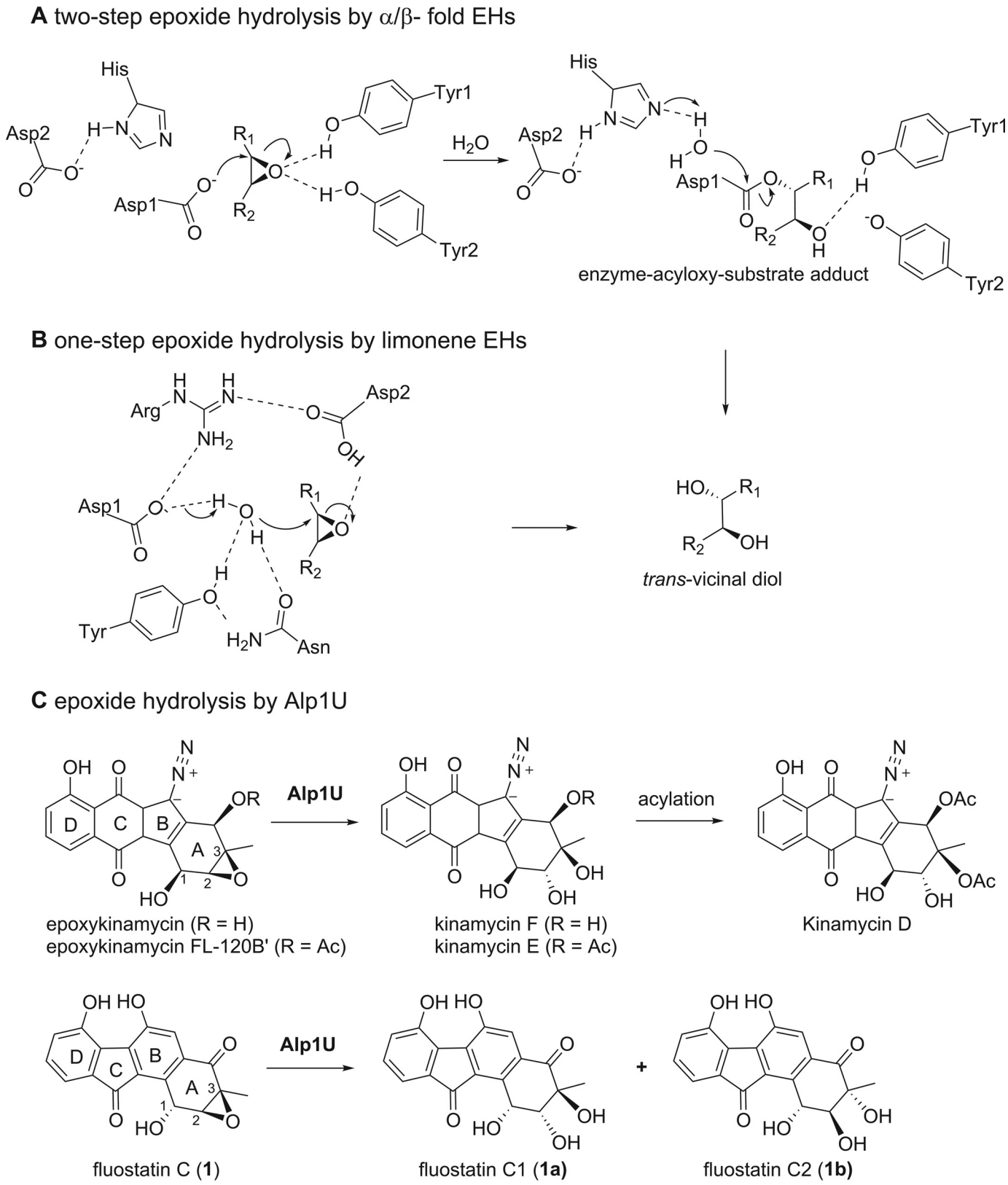

Figure 1. Classical epoxide hydrolase–catalyzed reactions. *A*, mechanism of the two-step epoxide hydrolysis; *B*, mechanism of the one-step epoxide hydrolysis; *C*, Alp1U-catalyzed epoxide hydrolysis with epoxykinamycins and FST C (**1**). Structures of FST C1 (**1a**) and C2 (**1b**) were determined in this study.

(FST) C (**1**) from *Micromonospora rosaria* (27, 28) as a substrate and catalyzes the epoxide hydrolysis to produce a pair of stereoisomers, FST C1 (**1a**) and FST C2 (**1b**). The origins of these stereoisomers were proposed to result from nonregioselective hydrolysis by nucleophilic attack at the C-2 and C-3 position of **1** (Fig. 1*C*) (29).

Herein, we determined the absolute stereochemistry of the two products FSTs C1 (**1a**) and C2 (**1b**) from Alp1U-catalyzed epoxide ring opening of FST C (**1**) and solved the X-ray crystal structure of Alp1U. An atypical oxirane oxygen hole is identified in Alp1U, consisting of three residues (Trp-186/Trp-187/Tyr-247) that are distinct from the Tyr/Tyr pair in classic α/β-EHs. The regioselectivity was improved for the epoxide ring opening of **1** in the single mutant Y247F to occur predominantly at C-3 and in the double mutant W187F/Y247F mainly at C-2. Single-crystal X-ray structures of these two Alp1U variants complexed with **1** were determined to help infer mechanistic insights into their opposite regioselectivities.

Results and discussion

Determination of the stereochemistry of epoxide ring–opening products

We have previously shown that Alp1U converts fluostatin C (**1**) to two stereoisomers, **1a** and **1b**, the structures of which have not yet been elucidated (29). Subsequently, compounds **1a** and **1b** were isolated from a large-scale enzymatic reaction with Alp1U and **1** to elucidate the structure. Both **1a** and **1b** had a molecular formula of $C_{18}H_{14}O_7$ (*m/z* 341.0672 $[M-H]^-$ for **1a**, *m/z* 341.0673 $[M-H]^-$ for **1b**, calcd. for 341.0667; Fig. S1). The NMR data for **1a** and **1b** (Fig. 2 and Figs. S1 and S2) showed high similarity to those of the previously characterized FST C (**1**) (28). The relatively more downfield shifts of the C-2 and C-3 (Table S1) in **1a** and **1b,** compared with the same carbons of **1**, suggested the presence of a vicinal diol subunit at C-2/C-3 in both compounds, instead of the epoxide moiety at C-2/C-3 in **1** (28).

The *trans* relative configuration of H-1 and CH_3-3 in **1a** was indicated by the NOESY correlation of OH-1 and H_3-12 (Fig. 2*A*). To determine the relative configuration of H-1 and H-2, a propylidene acetal derivative of **1a** (**1a-At**) was prepared (Fig. 2*A*). The *cis* relative configuration of the 1,2-diol moiety in **1a-At** was established by the markedly different proton chemical shifts of the isopropylidene methyl groups ($\Delta\delta_H$ 0.36) and the relatively small coupling constant between H-1 and H-2 ($^3J_{H\text{-}1,H\text{-}2}$ = 5.5 Hz) (Fig. 2*A*, Fig. S3, and Table S2) (30, 31). The NOESY correlation of H-2/OH-3 in **1a-At** confirmed the relative *trans* configuration of OH-2 and OH-3 (Fig. 2*A* and Fig. S3). Therefore, the relative configuration of the 1,2,3-triol moiety in **1a** was determined as (1*R**,2*R**,3*S**) in accordance with the configurations of **1a-At**. Considering that **1a** was a ring-opened product of 2,3-epoxide **1**, it thus must preserve the original (*R*) absolute configuration at C-1, so the absolute configuration of **1a** was assigned as (1*R*, 2*R*,3*S*). The *trans* relative configuration of H-1 and H-2 in **1b** was indicated by the NOESY correlation of H-1 and OH-2 and the large value of the $^3J_{H\text{-}1,\,H\text{-}2}$ coupling constant in methanol-d_4 (Table S3 and Fig. S4). The NOESY correlation of H-1 and H_3-12 was also observed in **1b** (Fig. 2*B* and Fig. S2), suggesting the *cis* axial orientation of H-1 and CH_3-3 and a *trans*-vicinal diol moiety at C-2/C-3 in **1b** (Fig. 2*B*). In accordance, the three hydroxyl groups adopted equatorial arrangement in the low-energy computed ωB97X/TZVP polarizable continuum model (PCM)/MeCN conformers of (1*R*,2*S*,3*R*)-**1b**, whereas H-1 and CH_3-3 were axial. The absolute configuration of **1b** was determined as (1*R*,2*S*,3*R*) based on the good agreement between the experimental and calculated electronic circular dichroism (ECD) spectra of (1*R*,2*S*,3*R*)-**1b** (Fig. 2*B*). To further confirm the absolute configuration of **1b**, we tried derivatization with *p*-bromobenzoyl that was reported to enhance crystallization (32). A pyridine derivative of **1b** (**1b-Py**) could be obtained as single crystals from the reaction system, and it was determined to have a (3*R*) configuration by X-ray diffraction analysis, with a Flack parameter of 0.04 (10) (Fig. 2*C*, Fig. S5, and Table S4, CCDC 2016594). This supports the (3*R*) absolute configuration in **1b**. Taken together, the structures of **1a** and **1b** suggest that the nucleophilic attack by Alp1U at C-2 of **1** produces **1a**, whereas **1b** derives from the attack at C-3.

Crystal structure of Alp1U reveals an atypical oxirane oxyanion hole

To learn more details about the catalytic mechanism of the Alp1U reaction, the ligand-free structure of N-terminal His_6-tagged Alp1U was determined to 2.45 Å, with four chains per asymmetric unit (Table 1 and Fig. S6). The four Alp1U chains form two dimers according to PISA calculation (33). Each chain takes the canonical α/β-hydrolase fold, comprising a catalytic domain (residues 27–166 and 251–319) linked to an α-helical cap (residues 167–250) (Fig. 3*A*). The 26 residues at the N terminus that share no sequence similarity to reported crystal structures of EHs are not resolved in the structure likely because of the flexibility of this region. A PDB database search of the Alp1U coordinates by the Dali server (34) reveals that Alp1U is most similar to a fluoroacetate dehalogenase (FAcD, PDB entry 3R3U, Z-score 38.5) (35). However, Alp1U shares a conserved overall fold (Z-score 38.2–25) with a batch of α/β-EHs, despite low identities in their amino acid sequences (<30%), including the extensively studied epichlorohydrin epoxide hydrolase (EchA) from *Agrobacterium radiobacter* AD1 (PDB entry 1EHY) (6), *Bm*EH from *Bacillus megaterium* ECU1001 (PDB entry 4IO0) (13), the human soluble epoxide hydrolase (sEH, PDB entry 4HAI) (36), and the bacterial virulence factor EH (cif) from *Pseudomonas aeruginosa* (PDB entry 5TND) (12) (Fig. S7). Structural alignment of Alp1U with these α/β-EHs reveals that the catalytic triad of classic EHs is conserved in Alp1U, consisting of residues Asp-137, His-300, and Asp-161 (Fig. 3*B*). We propose that Alp1U catalyzes a two-step epoxide ring–opening reaction as the classic α/β-EHs (Fig. 1*A*). In the first step, Asp-137 launches a nucleophilic attack at the epoxide carbon and forms a covalent alkyl-enzyme intermediate. In the second step, His-300 activates a water molecule, in cooperation with Asp-161, hydrolyzing the alkyl-enzyme intermediate to release the vicinal diol product and Asp-137.

However, the Alp1U active site is different from those of classic α/β-EHs in the key oxirane oxygen hole (Fig. 3*B*). The canonical oxirane oxygen hole of α/β-EHs contains two Tyr residues that play critical roles in the first catalytic step, by forming H-bonds with the epoxide oxygen and stabilizing the liberated oxirane oxyanion (Figs. 1*A* and 3*B*) (8, 14) However, Alp1U has only one of the two conserved tyrosines (Tyr-247), whereas the second Tyr is putatively replaced by a tryptophan (Trp-186)

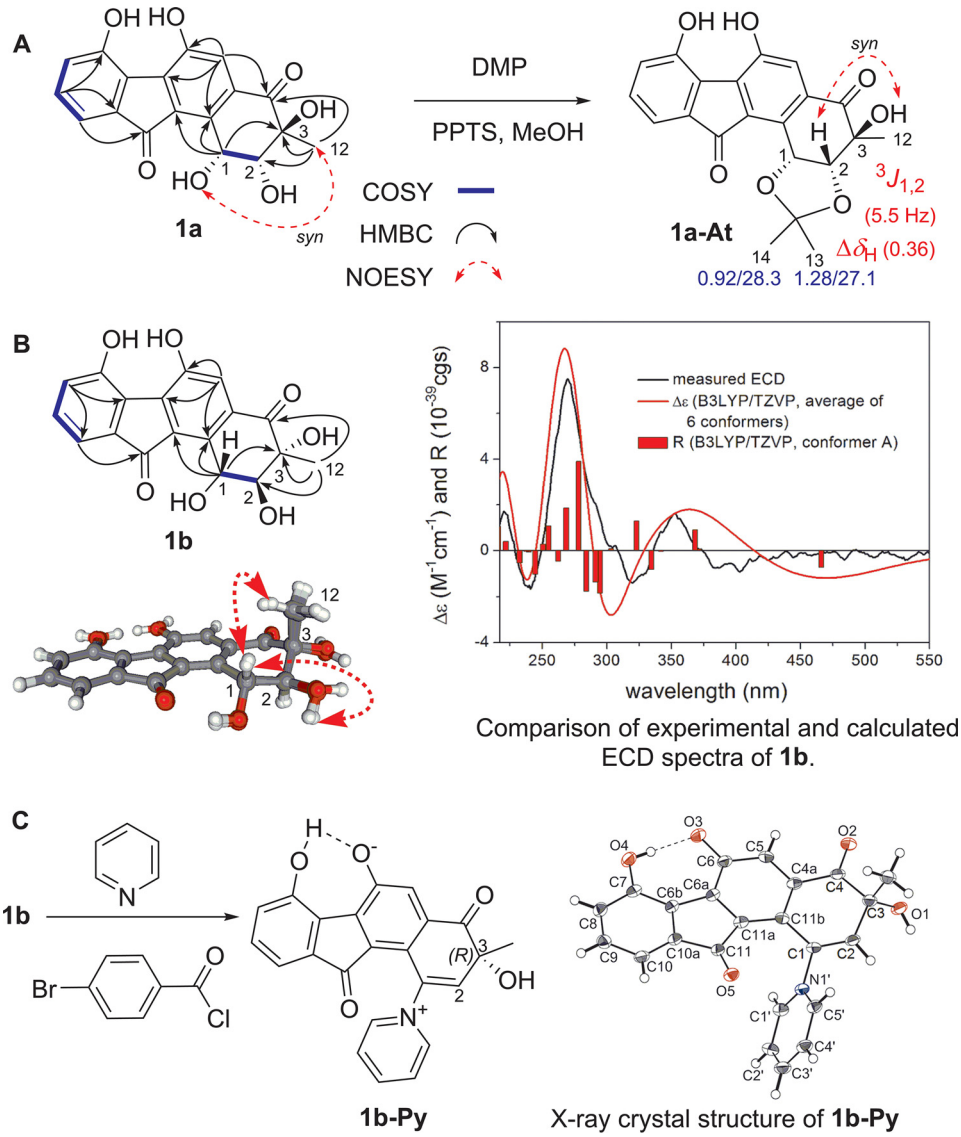

Figure 2. Establishment of stereochemistry of products 1a and 1b. *A*, key COSY, HMBC, and selected NOESY correlations for **1a**; chemical derivatization of **1a** to afford **1a-At**, and the NMR analysis of the derivative (**1a-At**). *B*, key COSY, HMBC, and selected NOESY correlations for 1b, geometries of the overlapped six lowest-energy ωB97X/TZVP PCM/MeCN conformers of (1*R*,2*S*,3*R*)-**1b**, and experimental ECD spectrum of **1b** (*black* line) compared with the B3LYP/TZVP PCM/MeCN//ωB97X/TZVP PCM/MeCN spectrum of (1*R*,2*S*,3*R*)-1b (*red line*). The *bars* represent rotational strength values for the lowest-energy solution conformers. *C*, a bromobenzoyl derivatization reaction of **1b** yields single crystals of the pyridine derivative 1b-Py with (3*R*) absolute configuration.

with its indole side chain being positioned for donating an H-bond to the oxirane oxygen (Fig. 3*B*). Also, the indole side chain of the adjacent Trp-187 is properly positioned to donate an H-bond to the oxirane oxygen (Fig. 3*B*). Therefore, the three residues Trp-186, Trp-187, and Tyr-247 putatively form an atypical oxirane oxygen hole in Alp1U to donor H-bonds to the epoxide oxygen.

Substrate regioselectivity by oxirane oxygen hole engineering

To confirm the proposed roles of the catalytic residues, the Alp1U mutants were generated by site-directed mutagenesis (Fig. 3*C*). As expected, three separate mutants, D137N, H300F, and H300G, completely abolished catalytic activity for **1** (Fig. 3*C*). The W186F mutant completely lost the activity, whereas the W187F mutant maintained the activity (Fig. 3*C*). It seems that Trp-186, rather than Trp-187, is required catalytically to donate an H-bond to the oxirane oxygen in **1**. Subsequently, the W186Y mutant was made to mimic the classic oxirane oxygen hole in EHs (10). However, W186Y showed no activity (Fig. 3*C*), likely because the side chain of Tyr-186 could not properly orient to interact with the oxirane oxygen.

It should be noted that a histidine (His-115) forms the oxirane oxygen hole with Tyr-219 in the bacterial virulence factor EH cif (Fig. 3*B*) (37), and a W186H mutant was also constructed. However, the W186H mutant only showed trace catalytic activity for the epoxide ring opening of **1** (Fig. 3*C*). The conserved Tyr-247 was expected to assist the epoxide ring–opening reaction by donating an H-bond to the oxirane oxygen. Surprisingly, the Y247F mutant retained most activity but selectively produced **1b** (98%), preferring a nucleophilic attack at C-3 (Fig. 3, *C* and *D*). The substrate conversion rates of W187F and Y247F suggest that neither Trp-187 nor the

Table 1

Crystal parameters, data collection, and refinement statistics

Statistics for the highest-resolution shell are shown in parentheses. RMSD, root mean square deviation.

	Alp1U	$Alp1U_{Y247F}$/**1**	$Alp1U_{W187F/Y247F}$/**1**
PDB ID	6KXR	6KXH	7CLZ
Wavelength (Å)	0.97894	0.97853	0.97853
Resolution range (Å)	70.19–2.45 (2.54–2.45)	31.98–1.78 (1.84–1.78)	44.7–2.1 (2.18–2.1)
Space group	P 21 21 21	P 21 21 21	P 21 21 21
Unit cell	a = 97.09, b = 101.58, c = 117.42, $\alpha = \beta = \gamma = 90$	a = 97.48, b = 101.56, c = 117.48, $\alpha = \beta = \gamma = 90$	a = 96.66, b = 100.21, c = 117.45, $\alpha = \beta = \gamma = 90$
Total reflections	86,069 (8505)	119,917 (11,484)	134,284 (13,302)
Unique reflections	43,063 (4255)	111,803 (10,937)	67,180 (6651)
Multiplicity	2.0 (2.0)	1.1 (1.1)	2.0 (2.0)
Completeness (%)	99.35 (99.51)	99.88 (99.25)	99.98 (99.97)
Mean $I/\sigma(I)$	13.73 (3.21)	16.18 (2.99)	8.58 (2.95)
Wilson B-factor	46.68	26.43	31.22
R-merge	0.02819 (0.2004)	0.112(0.756)	0.03037 (0.188)
Reflections used for R-free (%)	4.77	4.97	5.20
R-work	0.1687 (0.2150)	0.1712 (0.2162)	0.1932 (0.2190)
R-free	0.2344 (0.3197)	0.2061 (0.2691)	0.2468 (0.3006)
No. of nonhydrogen atoms	9233	10,016	9570
Macromolecules	9097	9125	9078
Ligands	9	117	118
Water	127	774	354
Protein residues	1170	1173	1172
RMSD (bonds) (Å)	0.008	0.007	0.009
RMSD (angles) (degrees)	1.11	1.14	1.22
Ramachandran favored (%)	96	97	97
Ramachandran outliers (%)	0.34	0.34	0.34
Clashscore	10.12	5.81	7.51
Average B-factor	45.30	34.10	32.40
Macromolecules	45.40	33.70	32.30
Ligands	49.50	36.80	39.30
Solvent	39.30	38.50	33.50

conserved Tyr-247 in Alp1U is a key H-bond donor to stabilize the oxirane oxygen of **1**. To verify this hypothesis, the W187F/Y247F double mutant was constructed. Unexpectedly, the $Alp1U_{W187F/Y247F}$ mutant selectively produced **1a** (94%) as a result of preferentially attacking at C-2. These observations are in sharp contrast to previous reports that classic α/β-EHs slightly lost the activity if one of the two catalytic Tyr residues in the oxirane oxygen hole was mutated and became completely inactive if both Tyr residues were mutated (7). To the best of our knowledge, such significant regioselectivity improvement and switch by mutated residues of the oxirane oxygen hole in Alp1U are unprecedented in EHs that catalyze epoxide ring–opening reactions.

Structural basis for the switch in regioselectivity

To investigate how the Alp1U mutants achieved the regioselectivity, the crystal structures of the $Alp1U_{Y247F}$ (1.78 Å) and $Alp1U_{W187F/Y247F}$ (2.1 Å) mutants were determined in complex with the substrate FST C (**1**), by soaking with an excess of **1** (Table 1). In both crystal structures, the clear electron density of **1** is observed (Fig. 4*B* and Fig. S8). Superposition reveals that the two structure complexes are essentially identical to the apo-Alp1U structure (Fig. S9). The catalytic cavity of Alp1U forms a deep groove, with a negatively charged surface, which binds the substrate FST C (**1**) (Fig. 4*A*). FST C (**1**) is bound to Alp1U mainly by direct and water-mediated hydrogen bond networks (Fig. 4*B*). The OH-1 hydroxyl group of **1** orients to the inner side of the active site. Therefore, the *O*-acyl or *O*-methyl derivatization at OH-1 could hamper FSTs from entering the Alp1U active site for a steric crowding effect. This might explain our previously reported phenomenon that Alp1U fails to convert FSTs containing an *O*-acyl or *O*-methyl group at the C1 position (29).

Similar binding patterns of **1** are observed in both structures of $Alp1U_{Y247F}$ and $Alp1U_{W187F/Y247F}$ in complex with **1** and suggest that Alp1U uses the same epoxide ring–opening mechanism as that of classic α/β-EHs (Fig. 4, *C–E*). In both structures (Fig. 4, *C* and *D*), the carboxyl side chain of Asp-137 locates just below the epoxide ring of **1**, ready for the nucleophilic attack. His-300 locates adjacent to Asp-137 and forms a hydrogen bond with Asp-161, consistent with its general role to activate one water molecule for hydrolyzing the covalent substrate-enzyme adduct and the subsequent release of Asp-137. The epoxide ring of FST C (**1**) is accommodated in the putative oxirane oxygen hole defined by the side chains of Trp-186, Trp-187, and Tyr-247 (Fig. S10). Trp-186 is perfectly positioned to synchronously protonate the epoxide oxygen, consistent with its critical role for the activity. The epoxide oxygen of **1** locates in hydrogen bond distance (Fig. 4*F*) to the indole N-H of Trp-187 (3.24 Å) and OH of Tyr-247 (2.81 Å). However, the N-H···O angle and O-H···O angle (Fig. 4*F*) are inappropriate to donate H-bonds, considering that the ideal X-H···Y angle for a hydrogen bond is generally linear or close to 180° (38). This may explain why the W187F and Y247F mutants retain the catalytic activity.

Structural alignments of Alp1U, $Alp1U_{Y247F}$/**1**, and $Alp1U_{W187F/Y247F}$/**1** complexes reveal highly overlapped Asp-137, His-300, Asp-161, and Tyr-247 but a slight displacement of Trp-186 and the adjacent Trp-187 (Fig. 4*F*). Structural comparison reveals that the substrate **1** in $Alp1U_{W187F/Y247F}$ adopts a ~20° anticlockwise rotation (Fig. 4*F*), compared with that in $Alp1U_{Y247F}$. We propose that the substrate rotation is caused by repulsive forces from the two hydrophobic side chains of

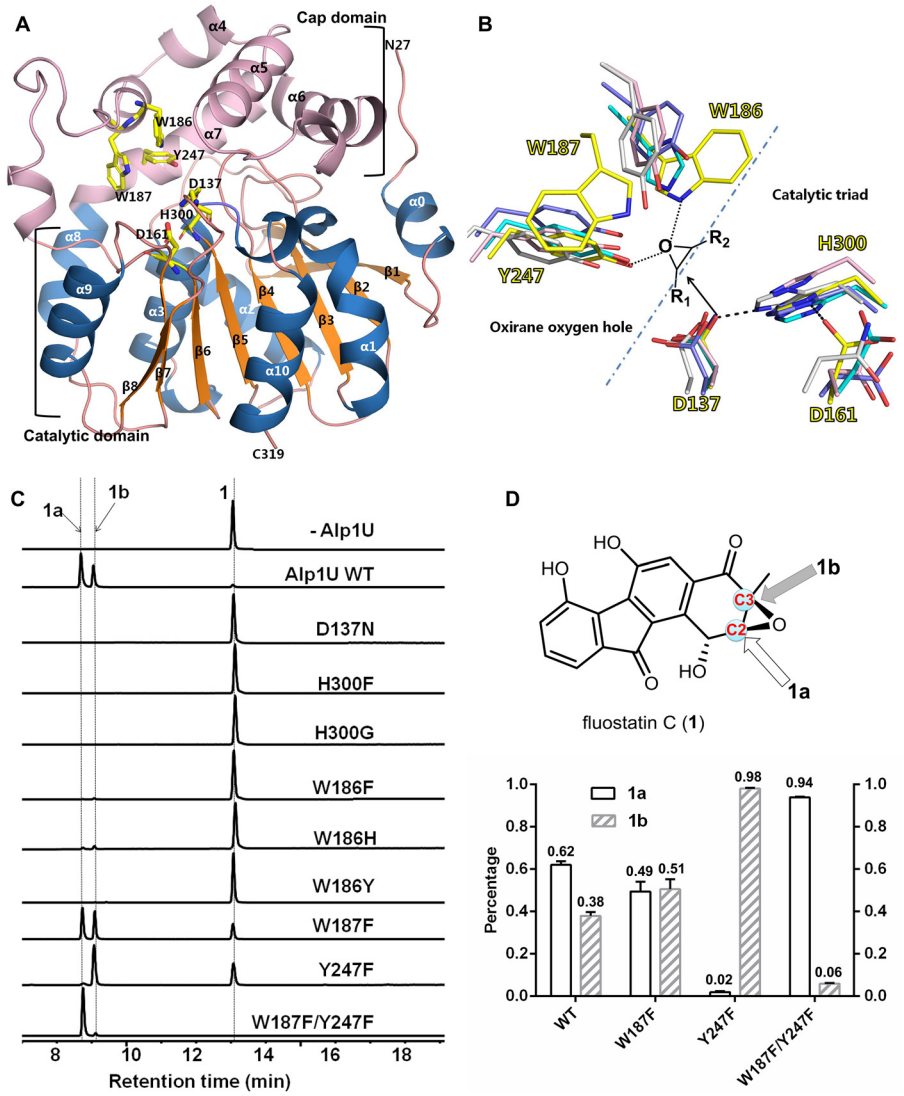

Figure 3. Crystal structure of Alp1U and characterization of catalytic residues. *A*, a *cartoon model* of the one Alp1U monomer. The cap domain (*pink*) and the catalytic domain (*blue* and *gold*) of one monomer are indicated. *B*, *close-up view* of Alp1U catalytic residues (*yellow sticks*) aligned with those of α/β-EHs including the epichlorohydrin epoxide hydrolase (EchA) from *A. radiobacter* AD1 (*slate sticks*), the *Bm*EH from *B. megaterium* ECU1001 (*gray*), human soluble epoxide hydrolase (sEH; *pink*), and the bacterial virulence factor EH (cif) from *P. aeruginosa* (*cyan*). *C*, HPLC traces for *in vitro* activity of Alp1U and mutants, using the substrate FST C (**1**). *D*, the regioselectivity switch of Alp1U toward **1**, through single and double site mutations, with each *in vitro* assay repeated three times.

Phe-247 and Phe-187 in $Alp1U_{W187F/Y247F}$. This rotation brings the carboxyl oxygen of Asp-137 significantly closer to C-2 of **1** in the $Alp1U_{W187F/Y247F}$/**1** complex (2.91 Å) than in the $Alp1U_{Y247F}$/**1** complex (3.18 Å). This new positioning likely directs the regioselective attack at C-2 of the epoxide ring to selectively produce **1a** (94%). This observation is consistent with previous studies describing the distances between the nucleophile and epoxide carbons as essential toward determining the regioselectivity of other EHs (14, 15, 20). However, the Y247F mutant prefers a regioselective attack at C-3 of **1** to produce **1b** (98%), despite the similar distances between the nucleophile Asp-137 and C-2 (3.18 Å) and between Asp-137 and the C-3 carbon (3.24 Å) in the $Alp1U_{Y247F}$/**1** complex. It is suggested from the $Alp1U_{Y247F}$/**1** complex that the hydrophobic effect of the phenyl side chain, introduced by the Y247F mutation, disfavors the carboxyl anion of Asp-137 to approach C-2 of **1** and largely reduces the preference for attack at C-2. Thus, $Alp1U_{Y247F}$ led to a regioselective attack at C-3. The C-3 selectivity of the Y247F mutant suggests that the regioselectivity for epoxide hydrolysis may not be solely determined by the distance of the interacting atoms, especially when the distances to both epoxide carbons are similar. Other parameters, such as hydrophobic effects, must be considered to account for the unexpected regioselectivity.

Conclusion

In this work, we identified that Alp1U structurally shows a conserved overall fold as classic α/β-EHs, but it features a unique triad (Trp-186/Trp-187/Tyr-247) to assemble an atypical oxirane oxygen hole that is usually defined by two residues of Tyr/Tyr for the canonical α/β-EHs. Mutation of residues in the atypical oxirane oxygen hole of Alp1U led to improved and switched regioselectivity for the epoxide hydrolysis of **1**. The

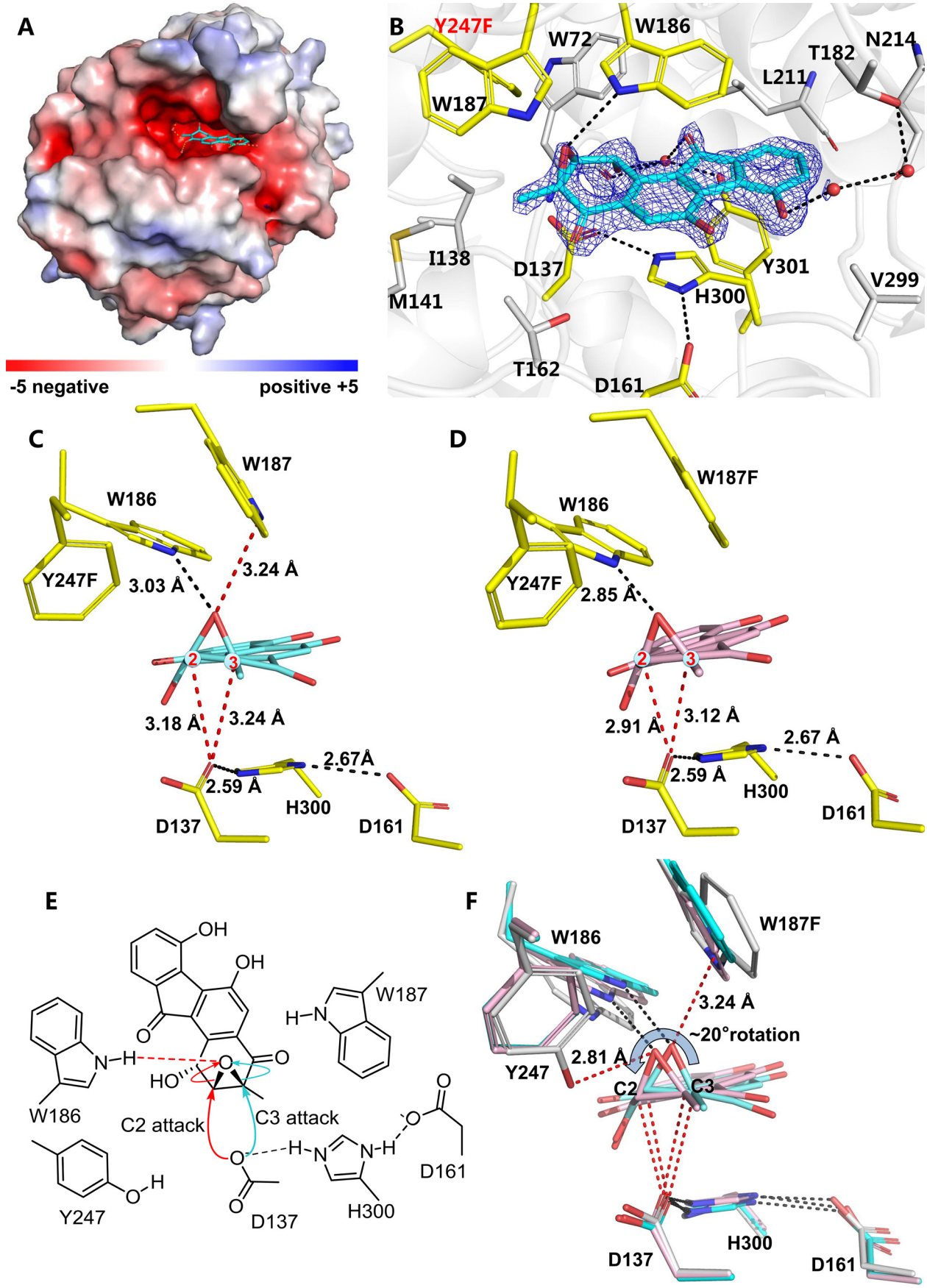
A
-5 negative
positive +5
B
Y247F
W72
W186
T182
N214
L211
W187
I138
D137
Y301
V299
M141
H300
T162
D161
C
W187
W186
Y247F
3.03 Å
3.24 Å
2
3
3.18 Å
3.24 Å
2.67Å
2.59 Å
H300
D137
D161
D
W187F
W186
Y247F
2.85 Å
2
3
2.91 Å
3.12 Å
2.67 Å
2.59 Å
H300
D137
D161
E
OH
OH
W187
H-N
O
N-H
HO
O
O
W186
C2 attack
C3 attack
O
H-N
N-H
O
D161
Y247
O-H
O
D137
H300
F
W186
W187F
3.24 Å
~20°rotation
2.81 Å
Y247
C2
C3
H300
D137
D161

single site mutant Y247F regioselectively attacks at C-3 (98%) of FST C (1) to form **1a**, the (1*R*,2*R*,3*S*)-isomer, whereas the double mutant W187F/Y247F prefers attacking regioselectively at C-2 (96%) to form the (1*R*,2*S*,3*R*)-**1b**. Crystal structures of the two mutants with distinctly different regioselectivities in complex with FST C (**1**) were determined to reveal slight conformation changes of the substrate and residues of the oxirane oxygen hole. These structural and mutagenesis studies of Alp1U and its mutants provided further insight into the factors governing the regioselectivity of α/β-EHs, which suggests that other parameters, such as hydrophobic effects, should be considered, in addition to the distance of the interacting atoms.

Experiment procedures

General materials

Chemicals and molecular biological reagents were purchased from standard commercial sources and used according to the manufacturers' recommendations. CD spectra were recorded on a Chirascan CD spectrometer (Applied Photophysics Co.). ^{1}H NMR, ^{13}C NMR, and two-dimensional NMR spectra were recorded on Bruker 700 spectrometer with tetramethylsilane as the internal standard. High-resolution electrospray ionization mass spectrometric data were measured on a MaXis 4G UHR-TOFMS spectrometer (Bruker Daltonics Inc.). DNA primers used in this study are listed in Table S5.

Cloning, expression, and purification of Alp1U and variants

The cloning and overexpression of Alp1U were performed basically as reported previously (29). Briefly, the Alp1U coding sequence was amplified and subcloned into pET28a(+) vector with an N-terminal His_6 fusion tag. Site-directed mutagenesis of Alp1U was carried out according to the manufacturer's instructions (Fast Mutagenesis System, TransGen). The W187F/Y247F double mutant was constructed using the verified Y247F plasmid as template.

Alp1U and mutants were expressed in *Escherichia coli* BL21 (DE3) cells. For fermentation, a 1-liter culture using lysogeny broth medium supplemented with 0.1 mM kanamycin was grown at 37 °C until the OD_{600} reached 0.5−0.7 and then was induced with 0.1 mM isopropyl-β-D-1-thiogalactopyranoside and allowed to grow at 16 °C overnight. For purification, cells collected by centrifugation were resuspended in lysis buffer (50 mM Tris-HCl, 500 mM NaCl, 10% glycerol, pH 8.0), lysed by three passes through an ultrahigh-pressure JN-mini homogenizer machine (Guangzhou Juneng Nano&Bio Technology Co. Ltd., Guangzhou, China), and then centrifuged for 45 min at 11,000 rpm at 4 °C. His_6-tagged proteins were purified by Ni^{2+}-nitrilotriacetic acid–agarose (GE Healthcare, 17-5318-03) affinity chromatography. For crystallization, the target protein was subjected to further purification using Superdex 200 (buffer containing 20 mM Tris, pH 7.5, 200 mM NaCl, 1 mM DTT) and concentrated to ~20 mg ml^{-1} using an Ultracel 30K filter (Millipore). The purity of WT Alp1U and variants was analyzed by SDS-PAGE (Fig. S11), and the final concentration was determined by a NanoDrop 8000 (Thermo Scientific).

In vitro enzyme assays

In vitro enzyme assays of recombinant Alp 1U and mutant variants were conducted in 100 μl of phosphate buffer (50 mM, pH 7.0) comprising 50 μM substrate and 5 μM enzyme. The reactions were incubated at 30 °C for 2 h. The reactions were terminated with an equal volume of ice-cold methanol. HPLC analysis of the enzyme reactions was carried out on the Agilent 1260 Infinity series instrument (Agilent Technologies Inc.) using a reversed-phase column (Phenomenex Luna, C18, 5 μm, 150 × 4.6 mm) with UV monitoring of the effluent at 304 nm using the following solvent system: solvent A, 10% acetonitrile in water supplemented with 0.1% formic acid; solvent B, 90% acetonitrile in water; elution profile: 5% B to 80% B (0–20 min), 100% B (21–24 min), 100% B to 5% B (24–25 min), 5% B (25–30 min); flow rate at 1 ml min^{-1}.

Isolation of 1a and 1b

An assay was scaled up and contained 10 μM recombinant Alp1U and 100 μM substrate **1** in 100 mM phosphate buffer (pH 7.0) of total volume 1.5 liters at 30 °C for 2 h. The reaction was extracted using butanone (3 × 1.5 liters), and the butanone was removed under vacuum. The remaining residue was dissolved in methanol followed by semipreparative HPLC using a Phenomenex C18 column (250 mm × 10 mm, 2.5 ml min^{-1}) with an isocratic solvent system (75% acetonitrile in water supplemented with 0.05% formic acid; flow rate at 2.5 ml min^{-1}) to yield compounds **1a** and **1b**.

Computational analysis

Mixed torsional/low-frequency mode conformational searches were done by the MacroModel version 10.8.011 software (Schrödinger, LLC, New York) using the Merck molecular force field with an implicit solvent model for $CHCl_3$. Geometry reoptimizations were carried out at the ωB97X/TZVP (39) level with the PCM for acetonitrile solvent. Time-dependent density functional theory electronic CD calculations were run with various functionals (B3LYP, BH&HLYP, CAM-B3LYP, PBE0) and the TZVP basis set as implemented in the Gaussian 09 package with the same or no solvent model as in the preceding DFT optimization step (40). ECD spectra were generated as sums of Gaussians with 1500–3000 cm^{-1} widths at half-height, using dipole velocity–computed rotational strength values (41).

Synthesis of the diacetate derivative of 1a

The conversion of triol compound **1a** to the isopropylidene derivative was carried out by following the previously reported

Figure 4. Crystal structures of Alp1U$_{Y247F}$ and Alp1U$_{W187F/Y247F}$ in complex with 1. *A*, the surface charge potential representation of Alp1U$_{Y247F}$ indicates the negatively charged groove-like active site. *B* and *C*, the binding mode of the Alp1U$_{Y247F}$ enzyme-substrate complex in different perspectives. Hydrogen bond interactions are indicated by *black dashed lines*. In Fig. 3*B*, the $2F_o - F_c$ maps are shown for FST C (**1**, *blue* mesh, contoured at 1.5σ). Catalytic triad and axirane oxyanion hole residues forming critical hydrogen bonds with **1** are shown as *yellow sticks*, whereas other peripheral residues are *colored gray*. *D*, binding pattern of Alp1Uw$_{187F/Y247F}$ in complex with **1**. *E*, proposed catalytic mechanism for the first nucleophilic attack of Alp1U. *F*, structural alignment of the WT Alp1U (*gray sticks*), Alp1U$_{Y247F}$/**1** (*cyan sticks*), and Alp1U$_{W187F/Y247F}$/**1** (*pink sticks*). Distances are indicated by *red dashed lines*.

procedure (42). A solution of **1a** (0.02 mmol) and pyridinium-*p*-toluenesulfonate (0.06 mmol) was dissolved in 2,2-dimethoxy propane (2 ml) and methanol (2 ml). The solution was stirred overnight at room temperature. The reaction was stopped with aqueous $NaHCO_3$ (5%, 1 ml) and extracted three times with CH_2Cl_2. The combined organic layers were reduced to dryness under vacuum, and the residue was purified by semipreparative HPLC to yield the diacetate derivative **1a** (**1a-At**, 3.5 mg) as a dark yellow powder. The structure of compound **1a-At** was confirmed by electrospray ionization MS and NMR analysis (Table S2 and Fig. S3).

Synthesis and X-ray crystallographic analysis of 1b pyridonide

To define the absolute configuration of **1b**, we reacted **1b** with *p*-bromobenzoyl chloride to convert it to its bromobenzoyl analog, improve the conditions for crystallization, and introduce a heavy atom. Following the previously reported method (32), the powdered **1b** (0.04 mmol) and *p*-bromobenzoyl chloride (0.21 mmol) and dimethylaminopyridine (0.12 mmol) are taken together and slowly dissolved with pyridine (4 ml) in a pear-shaped glass flask. The solution was stirred at room temperature for 24 h. The reaction was stopped after diluting with water and extracted with butanone (3 × 5 ml). The combined organic layers were reduced to dryness under vacuum, and light brown crystals appeared. A single crystal of **1b-Py** (Fig. 2*C*, Fig. S5, and Table S4) was diffracted on an XtaLAB AFC12 (RINC): κ single diffractometer with Cu Kα radiation (λ = 1.54184 Å). The crystal was kept at 104.5 ± 10 K during data collection. Using Olex2, the structure was solved with the ShelXT structure solution program using intrinsic phasing and refined with the ShelXL refinement package using least squares minimization. Crystallographic data have been deposited in the Cambridge Crystallographic Data Center with the deposition number CCDC 2016594.

Crystallization and structural elucidation of Alp1U and variants

Crystallization of Alp1U and its mutant variants were performed using the sitting-drop, vapor-diffusion method at 4 °C. The purified protein was mixed with an equal volume of reservoir solution (0.1 M MMT, pH 5.0, 25% PEG1500) purchased from Molecular Dimensions ltd. To obtain substrate-bound complex structure, the crystals of $Alp1U_{Y247F}$ and $Alp1U_{W187F/Y247F}$ were soaked in crystallization solution added with 2 mM FST C (**1**) (10 min, 16 °C) and immediately transferred to liquid nitrogen for cryopreservation. The diffraction data sets were collected at the Shanghai Synchrotron Radiation Facility beamlines BL19U1 and BL17U and processed and scaled using HKL3000 or XDS. The initial structure model was built by the molecular replacement method using PHENIX, with the fluoroacetate dehalogenase (FAcD RPA1163, PDB entry 3R3U) from *Rhodopseudomonas palustris* CGA009 as a search model, and then refined using REFINE. The geometrical restraints and PDB files for FST C (**1**) were generated by the Grade webserver. COOT was used for model adjustments and structural alignments. The qualities of the final model were validated by MolProbity (Table 1). Structural diagrams were prepared using the program PyMOL (Schrödinger, LLC, New York).

Data availability

Data are contained in the article as well as the supporting material. The authors welcome collegial communications on any and all content in this article. Crystallographic data for Alp1U were deposited in the Protein Data Bank (PDB) with accession codes 6KXR (apo-Alp1U), 6KXH ($Alp1U_{Y247F}$/**1**), and 7CLZ ($Alp1U_{W187F/Y247F}$/**1**). Crystallographic data have been deposited in the Cambridge Crystallographic Data Center with the deposition number CCDC 2016594.

Acknowledgments—The Governmental Information-Technology Development Agency (KIFÜ) is acknowledged for CPU time. We thank the staff of beamlines BL17U1, BL18U1, and BL19U1 of the Shanghai Synchrotron Radiation Facility (China) for access and help with the X-ray data collection. We are grateful to Z. Xiao, C. Li, A. Sun, Y. Zhang, and X. Ma in the analytical facilities of SCSIO for recording spectroscopic data.

Author contributions—L. Z. and C. Z. conceptualization; L. Z., B. C. D., W. Z., A. M., and Z. F. data curation; L. Z., W. Z., A. M., Z. F., T. K., and C. Z. software; L. Z. and W. Z. formal analysis; L. Z., B. C. D., W. Z., and C. Z. funding acquisition; L. Z. and W. Z. validation; L. Z. and C. Z. investigation; L. Z., B. C. D., W. Z., and C. Z. writing-original draft; L. Z., W. Z., Y. Z., T. K., and C. Z. writing-review and editing; B. C. D., W. Z., and A. M. methodology; Z. F., C. Y., Y. Z., and C. Z. resources; C. Z. supervision; C. Z. project administration.

Funding and additional information—This work was supported in part by National Natural Science Foundation of China (NSFC) Grants 31820103003, 31700042, and 41676165; Chinese Academy of Sciences Grants QYZDJ-SSW-DQC004 and XDA13020302; Special Project for Introduced Talents Team of Southern Marine Science and Engineering Guangdong Laboratory (Guangzhou) Grant GML2019ZD0406; and Guangdong Province Grants GDME-2018C005 and 2019B030302004. T. K. and A. M. were supported by National Research Development and Innovation Office Grant K120181. B. C. D. was supported by the CAS-TWAS President's Ph.D. Fellowship.

Conflict of interest—The authors declare that they have no conflicts of interest with the contents of this article.

Abbreviations—The abbreviations used are: EH, epoxide hydrolase; FST, fluostatin; PDB, Protein Data Bank; PCM, polarizable continuum model; ECD electronic circular dichroism.

References

1. Thibodeaux, C. J., Chang, W. C., and Liu, H. W. (2012) Enzymatic chemistry of cyclopropane, epoxide, and aziridine biosynthesis. *Chem. Rev.* **112,** 1681–1709 CrossRef Medline
2. Meninno, S., and Lattanzi, A. (2016) Organocatalytic asymmetric reactions of epoxides: recent progress. *Chemistry* **22,** 3632–3642 CrossRef Medline

3. Lee, E. Y., and Shuler, M. L. (2007) Molecular engineering of epoxide hydrolase and its application to asymmetric and enantioconvergent hydrolysis. *Biotechnol. Bioeng.* **98,** 318–327 CrossRef Medline
4. Saini, P., and Sareen, D. (2017) An overview on the enhancement of enantioselectivity and stability of microbial epoxide hydrolases. *Mol. Biotechnol.* **59,** 98–116 CrossRef Medline
5. Borhan, B., Jones, A. D., Pinot, F., Grant, D. F., Kurth, M. J., and Hammock, B. D. (1995) Mechanism of soluble epoxide hydrolase: formation of an α-hydroxy ester-enzyme intermediate through Asp-333. *J. Biol. Chem.* **270,** 26923–26930 CrossRef Medline
6. Nardini, M., Ridder, I. S., Rozeboom, H. J., Kalk, K. H., Rink, R., Janssen, D. B., and Dijkstra, B. W. (1999) The X-ray structure of epoxide hydrolase from *Agrobacterium radiobacter* AD1: an enzyme to detoxify harmful epoxides. *J. Biol. Chem.* **274,** 14579–14586 CrossRef Medline
7. Rink, R., Spelberg, J. H. L., Pieters, R. J., Kingma, J., Nardini, M., Kellogg, R. M., Dijkstra, B. W., and Janssen, D. B. (1999) Mutation of tyrosine residues involved in the alkylation half reaction of epoxide hydrolase from *Agrobacterium radiobacter* AD1 results in improved enantioselectivity. *J. Am. Chem. Soc.* **121,** 7417–7418 CrossRef
8. Yamada, T., Morisseau, C., Maxwell, J. E., Argiriadi, M. A., Christianson, D. W., and Hammock, B. D. (2000) Biochemical evidence for the involvement of tyrosine in epoxide activation during the catalytic cycle of epoxide hydrolase. *J. Biol. Chem.* **275,** 23082–23088 CrossRef Medline
9. Hopmann, K. H., and Himo, F. (2006) Insights into the reaction mechanism of soluble epoxide hydrolase from theoretical active site mutants. *J. Phys. Chem. B* **110,** 21299–21310 CrossRef Medline
10. Widersten, M., Gurell, A., and Lindberg, D. (2010) Structure-function relationships of epoxide hydrolases and their potential use in biocatalysis. *Biochim. Biophys. Acta* **1800,** 316–326 CrossRef Medline
11. Nestl, B. M., Hammer, S. C., Nebel, B. A., and Hauer, B. (2014) New generation of biocatalysts for organic synthesis. *Angew. Chem. Int. Ed. Engl.* **53,** 3070–3095 CrossRef Medline
12. Hvorecny, K. L., Bahl, C. D., Kitamura, S., Lee, K. S. S., Hammock, B. D., Morisseau, C., and Madden, D. R. (2017) Active-site flexibility and substrate specificity in a bacterial virulence factor: crystallographic snapshots of an epoxide hydrolase. *Structure* **25,** 697–707.e4 CrossRef Medline
13. Kong, X. D., Yuan, S., Li, L., Chen, S., Xu, J. H., and Zhou, J. (2014) Engineering of an epoxide hydrolase for efficient bioresolution of bulky pharmaco substrates. *Proc. Natl. Acad. Sci. U. S. A.* **111,** 15717–15722 CrossRef Medline
14. Amrein, B. A., Bauer, P., Duarte, F., Janfalk Carlsson, A., Naworyta, A., Mowbray, S. L., Widersten, M., and Kamerlin, S. C. (2015) Expanding the catalytic triad in epoxide hydrolases and related enzymes. *ACS Catal.* **5,** 5702–5713 CrossRef Medline
15. Sun, Z. T., Wu, L., Bocola, M., Chan, H. C. S., Lonsdale, R., Kong, X. D., Yuan, S. G., Zhou, J. H., and Reetz, M. T. (2018) Structural and computational insight into the catalytic mechanism of limonene epoxide hydrolase mutants in stereoselective transformations. *J. Am. Chem. Soc.* **140,** 310–318 CrossRef Medline
16. Li, F. L., Kong, X. D., Chen, Q., Zheng, Y. C., Xu, Q., Chen, F. F., Fan, L. Q., Lin, G. Q., Zhou, J. H., Yu, H. L., and Xu, J. H. (2018) Regioselectivity engineering of epoxide hydrolase: near-perfect enantioconvergence through a single site mutation. *ACS Catal.* **8,** 8314–8317 CrossRef
17. Carlsson, A. J., Bauer, P., Ma, H., and Widersten, M. (2012) Obtaining optical purity for product diols in enzyme-catalyzed epoxide hydrolysis: contributions from changes in both enantio- and regioselectivity. *Biochemistry* **51,** 7627–7637 CrossRef Medline
18. Faber, K., and Orru, R. V. A. (2002) Hydrolysis of epoxides. in *Enzyme Catalysis in Organic Synthesis* (Drauz, K., and Waldmann, H., eds) pp. 579–608, Wiley-VCH Verlag GmbH, Weinheim, Germany
19. Li, C., Kan, T. T., Hu, D., Wang, T. T., Su, Y. J., Zhang, C., Chen, J. Q., and Wu, M. C. (2019) Improving the activity and enantioselectivity of PvEH1, a *Phaseolus vulgaris* epoxide hydrolase, for *o*-methylphenyl glycidyl ether by multiple site-directed mutagenesis on the basis of rational design. *Mol. Catal.* **476,** 110517 CrossRef
20. Hu, D., Zong, X. C., Xue, F., Li, C., Hu, B. C., and Wu, M. C. (2020) Manipulating regioselectivity of an epoxide hydrolase for single enzymatic synthesis of (*R*)-1,2-diols from racemic epoxides. *Chem. Commun.* **56,** 2799–2802 CrossRef Medline
21. Sun, Z., Lonsdale, R., Kong, X. D., Xu, J. H., Zhou, J., and Reetz, M. T. (2015) Reshaping an enzyme binding pocket for enhanced and inverted stereoselectivity: use of smallest amino acid alphabets in directed evolution. *Angew. Chem. Int. Ed. Engl.* **54,** 12410–12415 CrossRef Medline
22. Abdel-Latief, M., Garbe, L. A., Koch, M., and Ruther, J. (2008) An epoxide hydrolase involved in the biosynthesis of an insect sex attractant and its use to localize the production site. *Proc. Natl. Acad. Sci. U. S. A.* **105,** 8914–8919 CrossRef Medline
23. Lin, S., Horsman, G. P., Chen, Y., Li, W., and Shen, B. (2009) Characterization of the SgcF epoxide hydrolase supporting an (*R*)-vicinal diol intermediate for enediyne antitumor antibiotic C-1027 biosynthesis. *J. Am. Chem. Soc.* **131,** 16410–16417 CrossRef Medline
24. Lin, S., Horsman, G. P., and Shen, B. (2010) Characterization of the epoxide hydrolase NcsF2 from the neocarzinostatin biosynthetic gene cluster. *Org. Lett.* **12,** 3816–3819 CrossRef Medline
25. Zheng, Q., Wang, S., Duan, P., Liao, R., Chen, D., and Liu, W. (2016) An alpha/beta-hydrolase fold protein in the biosynthesis of thiostrepton exhibits a dual activity for endopeptidyl hydrolysis and epoxide ring opening/macrocyclization. *Proc. Natl. Acad. Sci. U. S. A.* **113,** 14318–14323 CrossRef Medline
26. Wang, B., Guo, F., Ren, J. W., Ai, G. M., Aigle, B., Fan, K. Q., and Yang, K. Q. (2015) Identification of Alp1U and Lom6 as epoxy hydrolases and implications for kinamycin and lomaiviticin biosynthesis. *Nat. Commun.* **6,** 7674 CrossRef Medline
27. Baur, S., Niehaus, J., Karagouni, A. D., Katsifas, E. A., Chalkou, K., Meintanis, C., Jones, A. L., Goodfellow, M., Ward, A. C., Beil, W., Schneider, K., Süssmuth, R. D., and Fiedler, H. P. (2006) Fluostatins C-E, novel members of the fluostatin family produced by *Streptomyces* strain Acta 1383. *J. Antibiot.* **59,** 293–297 CrossRef Medline
28. Zhang, W., Liu, Z., Li, S., Lu, Y., Chen, Y., Zhang, H., Zhang, G., Zhu, Y., Zhang, G., Zhang, W., Liu, J., and Zhang, C. (2012) Fluostatins I-K from the South China Sea-derived micromonospora rosaria SCSIO N160. *J. Nat. Prod.* **75,** 1937–1943 CrossRef Medline
29. Huang, C., Yang, C., Zhang, W., Zhang, L., De, B. C., Zhu, Y., Jiang, X., Fang, C., Zhang, Q., Yuan, C. S., Liu, H. W., and Zhang, C. (2018) Molecular basis of dimer formation during the biosynthesis of benzofluorene-containing atypical angucyclines. *Nat. Commun.* **9,** 2088 CrossRef Medline
30. Hoshino, S., Okada, M., Wakimoto, T., Zhang, H., Hayashi, F., Onaka, H., and Abe, I. (2015) Niizalactams A–C, multicyclic macrolactams isolated from combined culture of *Streptomyces* with mycolic acid-containing bacterium. *J. Nat. Prod.* **78,** 3011–3017 CrossRef Medline
31. Nagle, D. G., and Gerwick, W. H. (1994) Structure and stereochemistry of constanolactones A-G, lactonized cyclopropyl oxylipins from the red marine alga *Constantinea simplex*. *J. Org. Chem.* **59,** 7227–7237 CrossRef
32. Sy-Cordero, A. A., Day, C. S., and Oberlies, N. H. (2012) Absolute configuration of isosilybin A by X-ray crystallography of the heavy atom analogue 7-(4-bromobenzoyl)isosilybin A. *J. Nat. Prod.* **75,** 1879–1881 CrossRef Medline
33. Krissinel, E., and Henrick, K. (2007) Inference of macromolecular assemblies from crystalline state. *J. Mol. Biol.* **372,** 774–797 CrossRef Medline
34. Holm, L. (2019) Benchmarking fold detection by DaliLite v.5. *Bioinformatics* **35,** 5326–5327 CrossRef Medline
35. Chan, P. W., Yakunin, A. F., Edwards, E. A., and Pai, E. F. (2011) Mapping the reaction coordinates of enzymatic defluorination. *J. Am. Chem. Soc.* **133,** 7461–7468 CrossRef Medline
36. Pecic, S., Pakhomova, S., Newcomer, M. E., Morisseau, C., Hammock, B. D., Zhu, Z. X., Rinderspacher, A., and Deng, S. X. (2013) Synthesis and structure-activity relationship of piperidine-derived non-urea soluble epoxide hydrolase inhibitors. *Bioorg. Med. Chem. Lett.* **23,** 417–421 CrossRef Medline
37. Bahl, C. D., and Madden, D. R. (2012) *Pseudomonas aeruginosa* Cif defines a distinct class of α/β epoxide hydrolases utilizing a His/Tyr ring-opening pair. *Protein Pept. Lett.* **19,** 186–193 CrossRef Medline

38. Shahi, A., and Arunan, E. (2016) Why are hydrogen bonds directional? *J. Chem. Sci*. **128,** 1571–1577 CrossRef
39. Chai, J. D., and Head-Gordon, M. (2008) Systematic optimization of long-range corrected hybrid density functionals. *J. Chem. Phys.* **128,** 084106. CrossRef Medline
40. Frisch, M., Trucks, G., Schlegel, H., Scuseria, G., Robb, M., Cheeseman, J., Scalmani, G., Barone, V., Mennucci, B., and Petersson, G. (2010) *Gaussian 09*, revision B.01, Gaussian Inc., Wallingford, CT
41. Stephens, P. J., and Harada, N. (2010) ECD cotton effect approximated by the Gaussian curve and other methods. *Chirality* **22,** 229–233 CrossRef Medline
42. Zhang, W., Li, S., Zhu, Y., Chen, Y., Chen, Y., Zhang, H., Zhang, G., Tian, X., Pan, Y., Zhang, S., Zhang, W., and Zhang, C. (2014) Heronamides D-F, polyketide macrolactams from the deep-sea-derived *Streptomyces* sp. SCSIO 03032. *J. Nat. Prod*. **77,** 388–391 CrossRef Medline